A&A 488, 235–244 (2008)
DOI: 10.1051/0004-6361:200809770

Astronomy & Astrophysics

Spatially resolved H_2 emission from the disk around T Tau N*

M. Gustafsson[1], L. Labadie[1], T. M. Herbst[1], and M. Kasper[2]

[1] Max-Planck-Institute for Astronomy, Königstuhl 17, 69117 Heidelberg, Germany
e-mail: [gustafsson;labadie;herbst]@mpia.de
[2] European Southern Observatory, Karl-Schwarzschild-Str. 2, 85748 Garching, Germany
e-mail: mkasper@eso.org

Received 12 March 2008 / Accepted 18 June 2008

ABSTRACT

Context. Molecular hydrogen is the main constituent of circumstellar disks and could be an important tracer for the evolution and structure of such disks. So far, H_2 has only been detected in a few disks and only through spectroscopic observations, resulting in a limited knowledge of the spatial distribution of the H_2 emitting gas.
Aims. We report the detection of quiescent H_2 emission in a spatially resolved ring-like structure within 100 AU of T Tau N. We present evidence to show that the emission most likely arises from shocks in the atmosphere of a nearly face-on disk around T Tau N.
Methods. Using high spatial resolution 3D spectroscopic *K*-band data, we trace the spatial distribution of several H_2 NIR rovibrational lines in the vicinity of T Tau N. We examine the structure of the circumstellar material around the star through SED modeling. Then, we use models of shocks and UV+X-ray irradiation to reproduce the H_2 line flux and line ratios in order to test how the H_2 is excited.
Results. We detect weak H_2 emission from the $v = 1{-}0$ S(0), S(1), Q(1) lines and the $v = 2{-}1$ S(1) line in a ring-like structure around T Tau N between 0.″1 (∼15 AU) and 0.″7 (∼100 AU) from the star. The $v = 1{-}0$ S(0) and $v = 2{-}1$ S(1) lines are detected only in the outer parts of the ring structure. Closer to the star, the strong continuum limits our sensitivity to these lines. The total flux of the $v = 1{-}0$ S(1) line is 1.8×10^{-14} erg s^{-1} cm^{-2}, similar to previous measurements of H_2 in circumstellar disks. The velocity of the H_2 emitting gas around T Tau N is consistent with the rest velocity of the star, and the H_2 does not seem to be part of a collimated outflow. Both shocks impinging on the surface of a disk and irradiation of a disk by UV-photons and X-rays from the central star are plausible candidates for the H_2 excitation mechanism. However, irradiation should not create a large degree of excitation at radii larger than 20 AU. Most likely the H_2 emission arises in the atmosphere of a flared disk with radius 85–100 AU and mass 0.005–0.5 $M_\odot$, where the gas is excited by shocks created when a wide-angle wind impinges on the disk. The H_2 emission could also originate from shock excitation in the cavity walls of an envelope, but this requires an unusually high velocity of the wide-angle wind from T Tau N.

Key words. stars: winds, outflows – stars: circumstellar matter – stars: emission-line, Be – stars: pre-main sequence – infrared: stars

1. Introduction

The study of circumstellar disks around young stars is essential to understanding their evolution from gaseous disks to planetary systems. In this paper, we examine the spatial distribution of molecular hydrogen, the main constituent of disks around young stars. Disks have been observed in a wide range of wavelengths ranging from optical to millimeter, although only a few studies have concentrated on the H_2 component. Many investigations have focused on the broad band spectral energy distribution, which reflects the disk geometry and the structure of the dust content. Disks have also been observed more directly via optically thick dust lanes blocking the scattered light from young stars, and as near-infrared images of the scattered light of the disk itself (e.g. McCabe et al. 2002; Weinberger et al. 2002). Molecular line emission from species such as CO or HCO^+ is also used as a tracer for disks. The use of such tracers is, however, subject to some uncertainty. Heavy element molecules may freeze out on dust grains, which likely settle to the midplane of the disk and/or get bound in larger rocks or planetesimals. Thus, molecules such as CO can become undetectable even if the disk still exists.

1.1. Molecular hydrogen in disks

Examining the H_2 content in disks has many advantages. Hydrogen and helium are the last parts of the gas to be bound up when planets form, and will therefore remain in the disk after CO and dust have become undetectable. Observations of molecular hydrogen directly trace the gas mass of the disk without making assumptions about the dust-to-gas or CO-to-H_2 ratios. Furthermore, molecular hydrogen will remain in the surface layers of the disk when the dust settles to the midplane and is more directly accessible to incoming light than the dust and heavier elements. As a result, H_2 may prove to be a better tracer for exploring the evolution and structure of circumstellar disks, since it may be observable for a longer period of time.

Direct observations of H_2 in disks have been undertaken by several groups. We focus here on the observations of the IR rovibrational lines, although some studies have concentrated on pure rotational lines in the MIR (e.g. Lahuis et al. 2007) as well as fluorescent H_2 in the UV (e.g. Walter et al. 2003; Herczeg et al. 2006). Emission from the H_2 $v = 1{-}0$ S(1) line at 2.1218 μm has been detected in the disks of several T Tauri stars, classical as well as weak-line (Bary et al. 2003, 2008; Itoh et al. 2003; Weintraub et al. 2005; Ramsay Howat & Greaves 2007; Carmona et al. 2008). These detections are made through longslit spectroscopic observations, and they do not reveal much

* Based on observations collected at the European Southern Observatory, Paranal, Chile under the programme 60.A-9041(A).

about the spatial distribution of the molecular hydrogen, beyond indicating that the emitting gas is located within 50 AU of the central star. Chen et al. (1998) presented images of H_2 v = 1−0 S(1) emission from photoevaporating disks in Orion and showed that the emission arises on the disk surface. In this case, the disks were externally irradiated, and the H_2 emission was found from a region ∼200 AU in size.

In this paper, we present spatially resolved images of H_2 emission from a ring around T Tau N obtained with the integral field spectrograph SINFONI on the ESO-VLT. The presence of H_2 emission in the T Tau system has been known for decades, but this is the first time that the weak emission within 100 AU of T Tau N has been resolved and analyzed.

1.2. T Tau

T Tau is a triple star system with an age of ∼1 Myr (White & Ghez 2001). The binary component T Tau S, consisting of T Tau Sa and T Tau Sb (separation ∼0.″1), is currently ∼0.″7 south of T Tau N. All three stars are actively accreting and believed to host disks (Duchêne et al. 2005). T Tau S shows heavy extinction (A_V = 15), which is attributed to a circumbinary structure (Duchêne et al. 2005). Another possibility is that T Tau S is obscured by the disk around T Tau N (Hogerheijde et al. 1997; Beck et al. 2001).

T Tau N is a ∼2 $M_\odot$ star (White & Ghez 2001) and is believed to have a disk that is seen nearly face-on (Akeson et al. 1998). Based on photometric periodicity and assumed stellar radius, Herbst et al. (1997) derive an inclination of 19°. Stapelfeldt et al. (1998) suggest an outflow and disk with the axis at position angle 300° and with inclination of ∼45° in order to explain the morphology of scattered optical light. Akeson et al. (2002) find the inclination to be 20−40° from SED fitting.

This paper is organized as follows. In Sect. 2, we describe the observations and data reduction. In Sect. 3, we present the spatial distribution of molecular hydrogen around T Tau N and the velocity distribution of the gas. Section 4 discusses the geometry of the star-disk-envelope system and Sect. 5 examines the H_2 excitation mechanism. In Sect. 6, we consider the possible implications for T Tau S, and finally, we draw conclusions in Sect. 7.

2. Observations

T Tau was observed with the ESO-VLT as part of the SINFONI science verification program on the nights of 2004 October 30th and November 2nd. SINFONI is a near-infrared (NIR) integral field spectrograph working in combination with adaptive optics (Eisenhauer et al. 2003). Observations of the region around the T Tau triple star system were obtained in the K-band using the 3.″2 field of view optics (100 mas pixel scale) centered on the northern component. T Tau N (m_V = 9.6) itself was used as the guide star, producing diffraction limited spatial resolution. The 2D image on the sky was sliced into 32 slitlets which were then dispersed onto a 2k × 2k detector. The spectrograph provides a spectral resolution of 4000 in the K-band. The observations were carried out using a five-point nodding pattern with individual exposure times of 3 s and 20 co-adds and a total integration time on source of 30 min. The nodding pattern was that of a box with one arcsecond width centered on T Tau N. The resulting mosaic has a field of view of approximately 4″. Sky frames with the same exposure times were obtained within the nodding cycle.

Data reduction and reconstruction of the 3D cubes were carried out using the SINFONI pipeline (version 1.3.0) provided by ESO. The 2D raw frames were corrected for sky background, flat field effects and optical distortions. Bad pixels and cosmic rays were identified and the frames were calibrated in wavelength. Then, the 3D cubes were constructed using calibration data of the positions and distances of the slitlets on the detector. The cubes within the nodding cycle were aligned spatially and coadded plane by plane to create the final mosaic. Since the total exposure time is less at the outer regions of the mosaic than in the centre we scaled the flux at all spatial points to an exposure time of 3 s. The final 3D cube stores the spatial information in the x- and y-directions and the spectral information along the z-direction. To improve the signal-to-noise ratio, each spectral plane was smoothed with a 3 by 3 boxcar in the spatial domain.

The B9 standard star Hip025657 was observed under the same conditions and similar airmass as T Tau and with the same instrumental setup, in order to correct for atmospheric absorption. The spectrum was extracted after the data had been reduced following the same recipe as for T Tau. The spectrum of Hip025657 is featureless except for Brγ in absorption. We removed this feature and replaced it by a linear fit to the surrounding continuum. Subsequently, the spectrum was divided by a blackbody function of T = 11 000 K and normalized. Dividing each spectrum of the science cube by the corrected standard star spectrum removed telluric absorption features in the T Tau spectra very effectively.

Flux calibration was also performed using Hip025657 (m_K = 7.443). The conversion factor between counts s^{-1} and erg s^{-1} cm^{-2} μm^{-1} sr^{-1} was found by dividing the K-band flux of the star (4.1×10^{-7} erg s^{-1} cm^{-2} μm^{-1} $\times$ $10^{-m_K/2.5}$, Campins et al. 1985) by the mean counts per second of the standard star spectrum within 1.94−2.45 μm and dividing by the pixel area in steradians.

3. Results

We show the spatial distribution of emission in the H_2 v = 1−0 S(1) rovibrational line at 2.12 μm in Fig. 1. The image is dominated by strong H_2 emission south of T Tau N, close to T Tau S. This emission feature was also detected by Herbst et al. (2007) and Beck et al. (2008). The origin of the strong emission south of T Tau N is believed to be outflows from one or more of the stellar components (Herbst et al. 2007) and will be the subject of a subsequent paper (Gustafsson et al., in preparation). In this paper, we focus on the weaker H_2 emission found very close to T Tau N. The weak feature is seen to extend all around the star in a ring-like structure. The morphology of the H_2 emission in our data is fully consistent with the map recently published by Beck et al. (2008). They also detected the weak ring-like structure although they did not mention it. Their data were obtained October 2005, which indicates that the emission feature is stable on at least a 1-year timescale.

A close-up of the immediate surroundings of T Tau N appears in Fig. 2. H_2 emission is found as close as 0.″1 arcsec (∼15 AU, assuming a distance of 140 pc) and is seen to extend out to ∼0.″7 (100 AU) from the star. We do not detect H_2 emission above the noise closer to the star than 0.″1. Molecular hydrogen does not appear in the spectrum of T Tau N (Fig. 3) and is an exclusively extended phenomenon.

Emission from other H_2 lines than the 1−0 S(1) transition has also been detected (Fig. 3). The 1−0 Q(1) line at 2.406 μm is found to have roughly the same spatial distribution as the

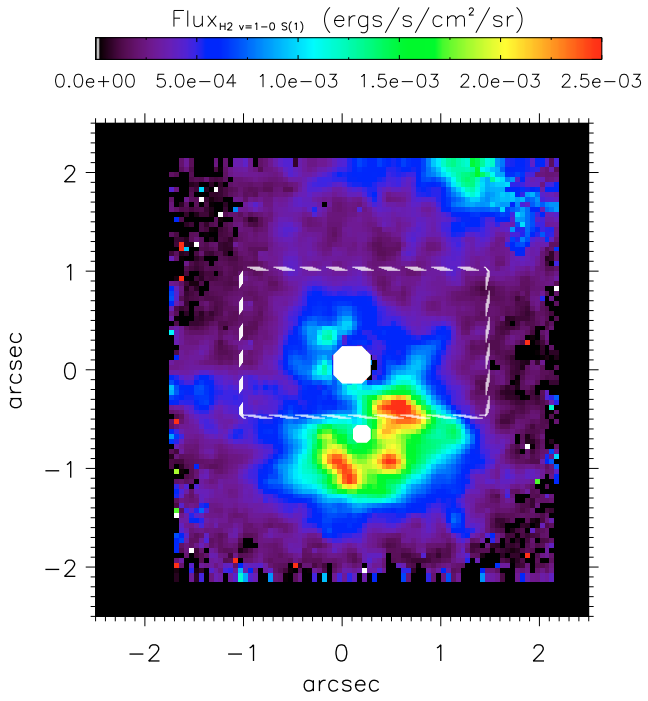

Fig. 1. H_2 $v = 1{-}0$ S(1) emission in the T Tauri system. The color scheme indicate the flux level in erg s^{-1} cm^{-2} sr^{-1}. The positions of T Tau N and T Tau S are marked with white circles. The white box outlines the close-up view of the ring-like structure around T Tau N shown in Fig. 2.

S(1) line. Other Q-branch lines are present as well, but the correction for atmospheric absorption is challenging in this spectral and spatial region and may introduce errors. The 1−0 S(0) line (2.2223 μm) also appears in the spectrum. This line is, however, weak and the powerful continuum emission from T Tau N limits the line detection at a level of 3σ above the noise level to pixels located in the outer ring structure at $r > 70$ AU. At larger radii, the S(0) emission shows a similar spatial distribution to the S(1) line. The $v = 2{-}1$ S(1) line (2.2447 μm) is tentatively detected at a 2σ level at a few locations in the outer region of the ring structure at $r > 80$ AU.

The total flux of the H_2 $v = 1{-}0$ S(1) in the structure is found by summing all light within a mask, the extent of which is shown in Fig. 2. We have chosen a rather conservative mask in order to avoid confusion with emission features that may have a different origin. Thus, the mask excludes regions where the emission is weaker than 4×10^{-4} erg s^{-1} cm^{-2} sr^{-1} as well as the strong emission region south-west of T Tau N which is most likely caused by an outflow from one of the T Tau S stars (Herbst et al. 2007). The total flux within the mask is $1.8 \pm 0.3 \times 10^{-14}$ erg s^{-1} cm^{-2}. The uncertainty is the formal uncertainty on the total flux calculated using the flux uncertainty in the pixels included in the sum. This uncertainty does not take into account that the estimated flux depends on the chosen mask and that the exact shape and extent of the ring-like structure is difficult to quantify because of other H_2 features nearby. We estimate that the uncertainty due to the mask may amount to 30%. The flux of the $v = 1{-}0$ Q(1) line and the upper limits to the flux of other H_2 lines appear in Table 1.

The total flux in the $v = 1{-}0$ S(1) line is similar to the amount of H_2 emission at the same radial velocity as the star detected in the circumstellar environment of other T Tauri stars, where it is believed to originate from disks within 100 AU (Bary et al. 2003, 2008; Weintraub et al. 2005; Ramsay Howat & Greaves 2007). The H_2 line flux previously measured in disks ranges from $7 \times 10^{-16}{-}1.5 \times 10^{-14}$ erg s^{-1} cm^{-2}.

In our data, we have full access to the spectral distribution of the emitting gas. Although SINFONI only has a spectral resolution of ~75 km s^{-1} in the K-band, it is possible to determine the peak position of the lines with much higher accuracy through line fitting. We have derived the radial velocity corresponding to every H_2 emitting position (see Fig. 2) by fitting a Gaussian profile to the unresolved line profiles on a pixel by pixel basis. The velocities in Fig. 2 have been corrected for the Earth's motion toward T Tau at the time of observation and are quoted with respect to the heliocentric velocity of T Tau N of 19.1 ± 1.2 km s^{-1} (Hartmann et al. 1986). The velocity map in Fig. 2 shows small velocity variations between −10 km s^{-1} and +10 km s^{-1} with respect to the intrinsic velocity of T Tau N within the ring structure. These velocities are consistent with the data from Beck et al. (2008) who also measure velocities close to the systemic velocity at this location (see their Fig. 11). There is a tendency for a radial gradient with the velocities being positive (5−10 km s^{-1}) close to the star and negative (−5 km s^{-1}) further out. However, the uncertainty in the derived velocities are larger close to the star than further out due to the increased continuum emission in the inner region (Fig. 2). This makes any conclusion on the radial variation of velocities rather uncertain. There is no evidence of Keplerian rotation of the disk. However, if the inclination of the disk is the same as the star itself, ~20°, the radial velocity component of Keplerian rotation around a 2 $M_\odot$ star is only ~5 km s^{-1} at 10 AU and ~2 km s^{-1} at 100 AU. Such small velocity differences within the disk would be difficult to detect with the present data.

In order to improve the signal-to-noise ratio, we constructed a global H_2 profile of the ring-like structure by adding all spectral profiles of H_2 $v = 1{-}0$ S(1) emitting positions within the mask in Fig. 2. This also allows a direct comparison with previous spatially unresolved measurements of H_2 in the circumstellar environment of T Tauri stars. The global line profile appears in Fig. 4 together with a Lorentzian fit. The Lorentzian fitting function provides the best match to the instrumental profile of SINFONI which dominates the unresolved H_2 profile. The profile is seen to peak close to the rest velocity of T Tau N. From the Lorentzian fit we find the peak velocity to be -2.5 ± 2.1 km s^{-1} (1σ uncertainty). Considering the uncertainty in the rest velocity of T Tau N of 1.2 km s^{-1} (Hartmann et al. 1986), the velocity of the H_2 emission is consistent with the rest velocity of the star within the errors. The same was found to be true of the H_2 emission from disks around other stars (Bary et al. 2003, 2008; Ramsay Howat & Greaves 2007; Carmona et al. 2008).

4. Disk or outflow?

We now examine the origin of the H_2 emission around T Tau N. The ring-like shape of the emission can be created by several scenarios. We consider the following possibilities: 1) an outflow, 2) shocks created by a wide-angled wind hitting a disk or cavity walls, 3) a photo-evaporating wind from a disk viewed almost face-on (Hollenbach et al. 1994; Font et al. 2004), 4) a photodissociation region, or 5) UV/X-ray heating of a disk (Nomura et al. 2007). In this section, we consider the geometry of the system and in Sect. 5, we examine what excitation mechanisms can reproduce the H_2 line flux and ratios.

Outflows from T Tauri stars are known to be complex, often showing two velocity components with different spatial characteristics. Observations of both forbidden emission lines

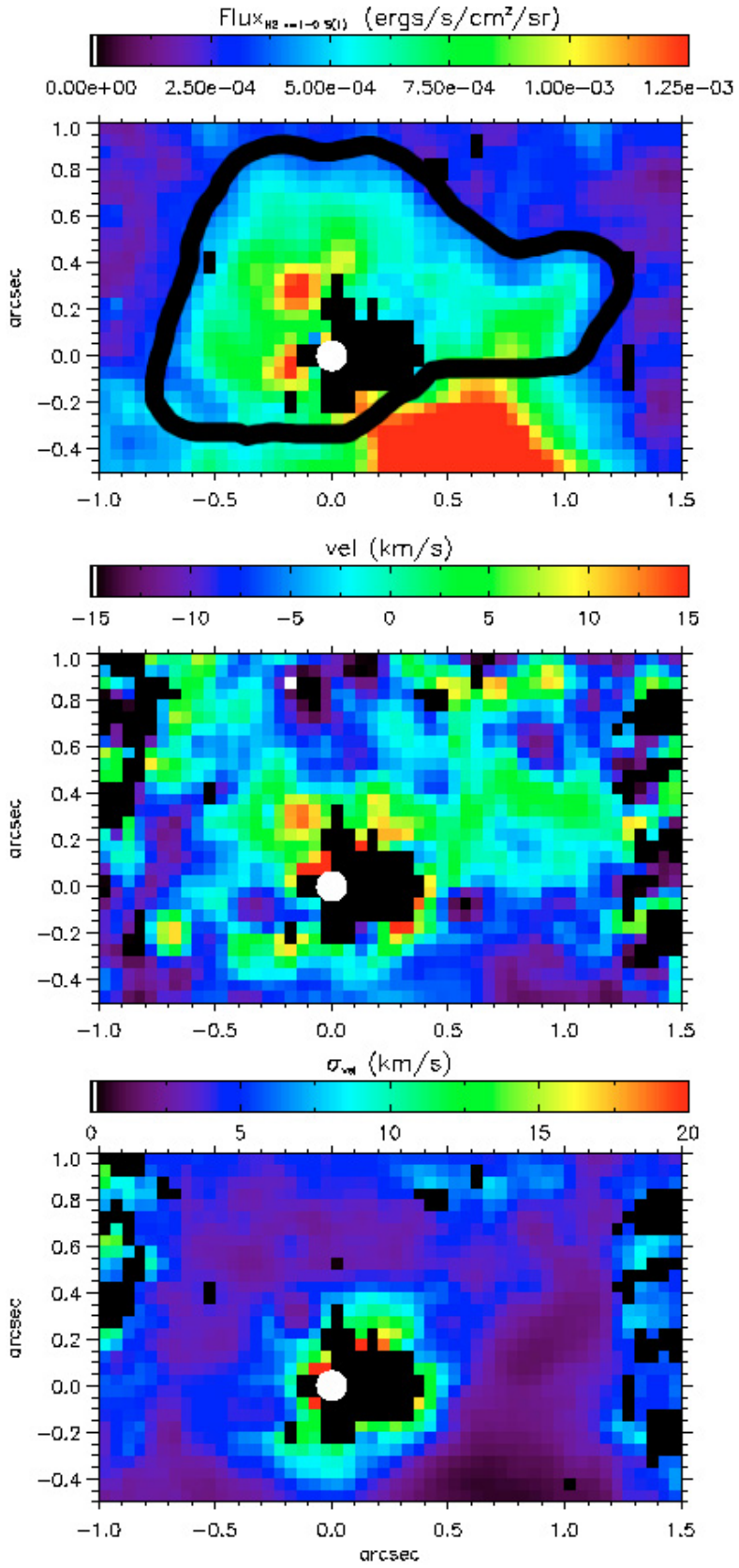

Fig. 2. *Top*: H_2 $v = 1{-}0$ S(1) emission surrounding T Tau N. The color scheme indicate the flux level in erg s^{-1} cm^{-2} sr^{-1}. Positions where no H_2 emission is detected are shown in black and the position of T Tau N is marked by a white circle. The mask outlining the region used for further analysis is indicated by the black line. The strong emission region south-west of T Tau N is excluded because it is most likely related to outflows from T Tau S (see text). *Centre*: the derived heliocentric radial velocity of the H_2 emission relative to the rest velocity of T Tau N. *Bottom*: uncertainties in the radial velocities.

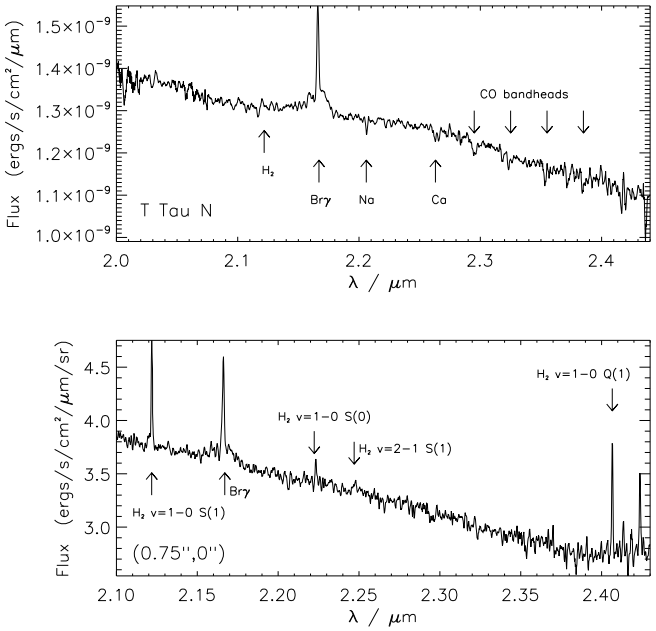

Fig. 3. *K*-band spectrum of T Tau N and of a pixel within the mask in Fig. 2 located (0.″75, 0) with respect to T Tau N. Brγ emission and photospheric absorption lines are seen in T Tau N. In the extended ring-like structure, only H_2 lines are detected. The Brγ line in the lower spectrum is contamination from the PSF of T Tau N and is not due to extended emission of Brγ.

Table 1. Total flux of H_2 lines within mask.

Line	λ (μm)	Flux (10^{-14} erg s^{-1} cm^{-2})	Ratio $F_{v=1-0S(1)}/F_{\rm line}$
$v = 1-0$ S(1)	2.1218	1.8 ± 0.3	1.0
$v = 1-0$ S(0)	2.2223	$<0.5^a$	>3.6
$v = 2-1$ S(1)	2.2477	$<0.6^a$	>3.0
$v = 1-0$ Q(1)	2.4066	1.9 ± 0.1	0.9

[a] 3σ upper limit.

(Bacciotti et al. 2000) and molecular hydrogen (Takami et al. 2006) have shown that outflows typically consist of a collimated high velocity (60–200 km s^{-1}) jet and a less collimated low velocity (0–30 km s^{-1}) component, i.e. a wide-angled wind. At first glance, the small line-of-sight velocities measured in the ring argue against a collimated jet. Although a jet viewed almost pole-on could create a circular emission feature, the velocities associated with such a jet are much higher than observed here. It is, however, possible that we see shocks from a wide-angle wind interacting with either the outer walls of a bi-conical cavity cleared out by the outflow or a flared disk (Figs. 5a or b). The existence of a cavity in an envelope around T Tau N was suggested by Momose et al. (1996) and the reflected light images of Stapelfeldt et al. (1998). In this picture, a wide-angle wind creates oblique shocks when interacting with the molecular environment. Oblique shocks result in low shock velocities, since it is only the normal component of the velocity with respect to the gas that is thermalized. Furthermore, the measured velocities will be even lower, since only the line-of-sight velocity is detected here.

Another possibility is that the emission is linked to irradiation of a nearly face-on disk around T Tau N (Fig. 5c). We proceed by investigating the circumstellar environment of T Tau N through spectral energy distribution (SED) modeling to find

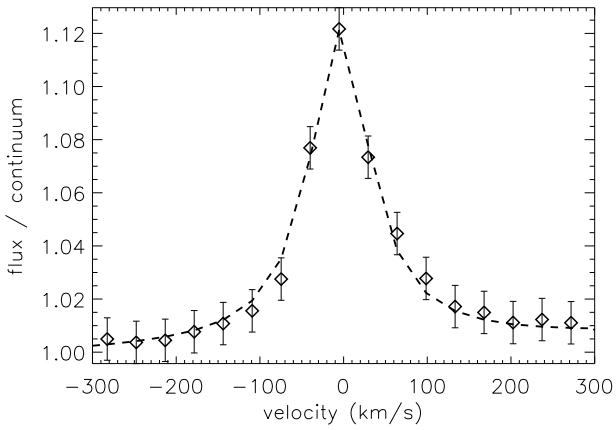

Fig. 4. H_2 $v = 1-0$ S(1) line profile integrated over the ring structure (diamonds with 1σ errorbars). Fitted Lorentzian (dashed line).

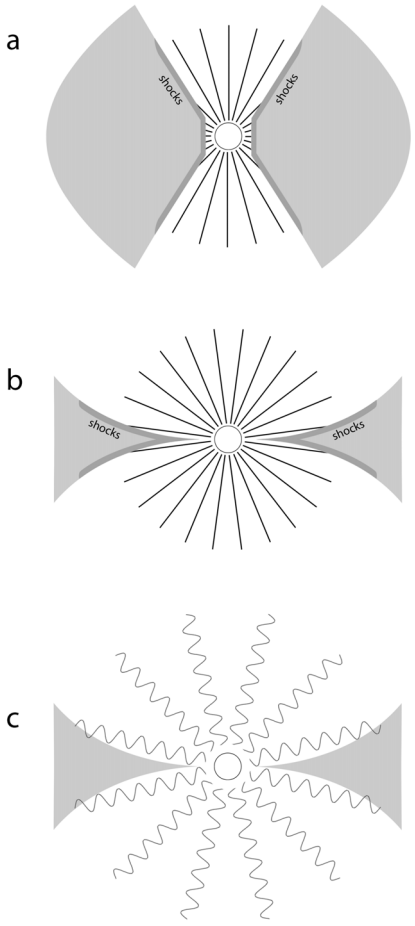

Fig. 5. Excitation scenarios in the T Tau N-disk-envelope system. **a)** A wide-angle outflow hits the walls of a cleared out cavity in the surrounding envelope, **b)** a wide-angle outflow impinges on a flared disk and creates shocks, **c)** UV + X-ray irradiation from T Tau N heats a flared disk.

evidence of the size of the disk and envelope. We use the pre-computed grid of radiative transfer models of Robitaille et al. (2007). Their models include contributions from a circumstellar accretion disk, an infalling envelope and an outflow cavity. The models span a wide range of parameter space. The SED is calculated for each set of model parameters for comparison with observational data. Using fluxes of T Tau N from the literature,

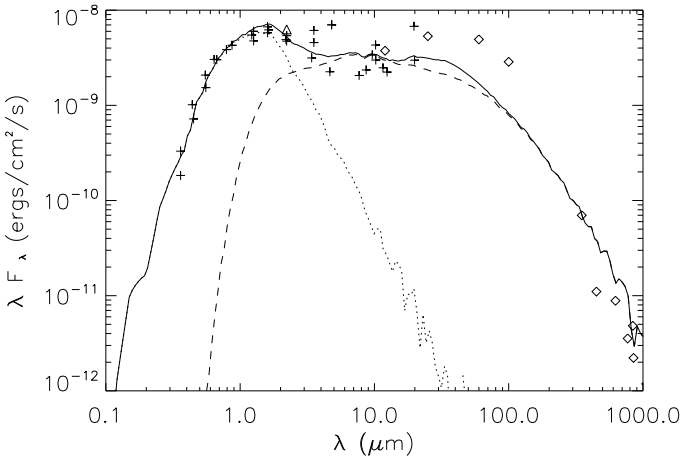

Fig. 6. Spectral energy distribution of T Tau N and model curves. The data points include those of this work and Herbst et al. (1997, 2007); Kenyon & Hartmann (1995); Hogerheijde et al. (1997); Weaver & Jones (1992); Andrews & Williams (2005); Beckwith & Sargent (1991). Plus-signs indicate resolved data of T Tau N, diamonds indicate where T Tau S and T Tau N are unresolved and the flux of T Tau S dominates. The *K*-band flux from this work is marked with a triangle. The model is found from fitting to data at $\lambda < 21$ μm where T Tau N and T Tau S are resolved. Solid line: total flux, dotted line: stellar flux, dashed line: disk flux.

we fit the optical and infrared data with the models in order to find the range of physical parameters that fit the SED best.

The SED appears in Fig. 6. The observations include those of Herbst et al. (1997, 2007); Kenyon & Hartmann (1995); Hogerheijde et al. (1997); Weaver & Jones (1992); Andrews & Williams (2005); Beckwith & Sargent (1991). T Tau N shows brightness varitations of 0.2 mag in the *K* and *L* bands (Beck et al. 2004), which can explain the spread in flux values that the various authors find. We have included measurements from different epochs at optical and infrared wavelengths, in order to average out the effect of this variability. In the model fit, we have only used data points at $\lambda < 21$ μm, for which the T Tau N component is resolved. At longer wavelengths, the north and south components of the T Tau triple system are unresolved and T Tau S dominates (Ghez et al. 1991). We assume that $A_V = 1.5$ (White & Ghez 2001).

The Robitaille grid resulted in a wide range of parameters that produced a reasonable fit to the SED. In order to further constrain the parameter space, we used the spectral information on T Tau N, a ~1 Myr old K0 star with $M \sim 2$ $M_\odot$, $T_{\rm eff} = 5200$ K (White & Ghez 2001). Thus, we chose to consider only those models in which the stellar parameters fall within the following ranges, $1.5 < M/M_\odot < 2.5$, 4000 K $< T_{\rm eff} <$ 6000 K, 0.1 Myr < age < 2 Myr. The best fit model which satisfies these criteria appears in Fig. 6. For the 50 models that best fit the data, only four models satisfy the stellar restrictions of T Tau N. These four models have the same values for all parameters except the inclination angle of the disk. The model parameters are listed in Table 2. The inclination is poorly determined, but is found to be less than 65°.

SEDs only contain a limited amount of information about the distribution of circumstellar material, and it is easy to overinterpret the results of model fitting. Nevertheless, our results show that the T Tau N system is consistent with an accreting star surrounded by a disk and torus-like envelope with an opening angle of ~45°. The disk is likely to have an outer radius of 85 AU consistent with the detection of H_2 at a radius of ~100 AU. It also

Table 2. SED model parameters.

Envelope accretion rate	10^{-7} $M_\odot$/yr
Cavity opening angle	47°
Disk mass	0.15 $M_\odot$
Disk outer radius	85 AU
Disk inner radius	0.3 AU
Flaring parameter, β	1.14
Disk accretion rate	10^{-6} $M_\odot$/yr
Disk inclination	<65°

shows a large degree of flaring. The inclination of the disk cannot be well constrained by the SED-modeling but is consistent with a low inclination of ~19°, as found by Herbst et al. (1997). The model is also consistent with the suggestion of Stapelfeldt et al. (1998) that an outflow at PA = 300° and inclination of 45° has blown out a cavity. Note that the disk accretion rate is higher than the observed accretion rate of (1.4–5.9) × 10^{-8} $M_\odot$ yr^{-1} based on the Brγ line strength (Beck et al. 2004). This is most likely due to inconsistencies in the radiative transfer models used in the Robitaille models, which systematically overestimate the accretion rate. This effect was already noted in Robitaille et al. (2007). Thus, the accretion rate inferred from the SED modeling should be considered with some caution.

Assuming optically thin emission, the mass of H_2 $v = 1$–0 S(1) emitting gas is (Bary et al. 2003)

$$M(\mathrm{H_2})_{v=1-0\ \mathrm{S(1)}} = 1.76 \times 10^{-20} \frac{4\pi F_{\rm line} D^2}{E_{v,J} A_{\rm line}} = 5 \times 10^{-10}\ M_\odot, \quad (1)$$

where $F_{\rm line}$ is the $v = 1$–0 S(1) flux, D the distance in pc, $E_{v,J}$ the upper level energy and $A_{\rm line}$ the Einstein A coefficient of the transition. Following Bary et al. (2003), we estimate the total disk mass by multiplying the $v = 1$–0 S(1) H_2 mass by a scaling factor of 10^7–10^9. This scaling factor was found by comparing the H_2 mass to masses derived from CO and (sub)millimeter continuum in disks around four T Tauri stars (GG Tau, LkCa 15, DoAr 21, TW Hya). This gives a disk mass of 0.005–0.5 $M_\odot$. Note that the most likely disk mass of 0.15 $M_\odot$ estimated from the SED modeling falls within this range. Analysis of HCO^+ and millimeter continuum data indicates that the disk mass around T Tau N is 10^{-3}–4×10^{-2} $M_\odot$ (Hogerheijde et al. 1997; Akeson et al. 1998), suggesting that the actual disk mass is at the lower end of the simple mass estimate based on the H_2 mass.

These arguments suggest that T Tau N has a flared disk with radius 85–100 AU and mass 0.005–0.5 $M_\odot$. We propose that the observed H_2 emission comes from the gaseous disk atmosphere or alternatively from the torus-like envelope that is also present around T Tau N according to the SED. The reason that T Tau N is not at the centre of the H_2 emission (Fig. 2) could be due to the fact that we do not see the disk-envelope system exactly face-on. An inclination of 20–40° would cause emission from a circular structure to appear elliptical. Assuming that we only see emission from the surface facing toward us projection effects would furthermore make the nearest side of a disk appear narrower than the farther side. This would shift the projected position of the central star away from the centre of emission. A detailed modeling of the spatial distribution of the emission is, however, outside the scope of this paper.

If the value of 85–100 AU reflects the true size of the disk, why has the disk not yet been detected in scattered light? The simplest explanation is that the disk is small ($r < 0\farcs7$) and the

flux contrast between the star and disk is large, making detection difficult. Infrared observations of scattered light from nearly face-on disks (circumstellar and circumbinary) around other T Tauri stars have shown that the total flux from a disk is only 1−2 percent of the stellar flux (McCabe et al. 2002; Weinberger et al. 2002). Stapelfeldt et al. (1998) and Mayama et al. (2006) observed reflected light in T Tau at optical and infrared wavelengths, respectively, but did not find evidence of the disk around T Tau N. However, Mayama et al. (2006) used a coronographic mask with a diameter of ∼0.″5−0.″6, which is only marginally smaller than the size of the disk found in this paper. The disk would therefore in any case be difficult to see in their data. The detection of the disk from the data of Stapelfeldt et al. (1998) could be compromised by artefacts arising from the PSF subtraction.

5. Excitation mechanism

After studying the location of the circumstellar material and the H_2 emitting gas, we now turn to the H_2 excitation mechanism. The near-infrared rovibrational lines of H_2 can be excited through different processes. The two main mechanisms are (i) shocks (Figs. 5a and b) and (ii) UV + X-ray radiation (Fig. 5c). In the former case, the H_2 molecules are thermally excited by the passing shock wave and the H_2 spectrum is characterized by a single excitation temperature. In the latter case, the UV and X-ray radiation may contribute both to the heating of the gas and to electronic excitation of H_2. The near-infrared H_2 emission may therefore contain a contribution from both thermal excitation as well as non-thermal radiative decay from excited electronic states (fluorescence). These two excitation mechanisms can be distinguished through both the line strengths and the line ratios of the observed H_2. Traditionally, the ratios $I_{v=1-0\ S(1)}/I_{v=1-0\ S(0)}$ and $I_{v=1-0\ S(1)}/I_{v=2-1\ S(1)}$ are used. These ratios also provide a diagnostic for whether the thermal or non-thermal contribution dominates, since higher vibrational bands, $v \geq 2$, are more densely populated by fluorescence than by thermal excitation. In the following, we will concentrate on the two excitation processes (i) shocks and (ii) UV + X-ray irradiation.

5.1. Shocks

In the first process, shocks, a super-Alfvenic shock wave rapidly heats the gas to temperatures of ∼1000−3000 K. The temperature reached depends on the velocity of the shock, as well as the pre-shock conditions in the ambient medium, such as density, magnetic field, chemistry etc. The $I_{v=1-0\ S(1)}/I_{v=2-1\ S(1)}$ ratio depends on the temperature, since the populations are assumed to be in local thermodynamic equilibrium (LTE). The higher the temperature, the larger the relative population in higher vibrational bands. We estimate the range of the $I_{v=1-0\ S(1)}/I_{v=2-1\ S(1)}$ ratio that shocks are able to produce considering the temperature range 1000−3000 K reached during the passing of the shock. For an optically thin transition, the line intensity is

$$I_{\rm line} = \frac{A_{\rm line} hc}{4\pi\lambda} N_{v,J}, \quad (2)$$

where $N_{v,J}$ is the population in the upper level denoted by the v and J quantum numbers, λ the wavelength, and $A_{\rm line}$ is the Einstein coefficient of the transition. We ignore extinction effects, since the differential extinction between the H_2 lines is small. In LTE, the level population is given by

$$N_{v,J} = \frac{N_{\rm tot}}{Z(T)} g_{v,J} \exp(-E_{v,J}/T), \quad (3)$$

where $N_{\rm tot}$ is the total column density, $Z(T)$ is the partition function, $g_{v,J}$ is the degeneracy of the level, $E_{v,J}$ is the level energy expressed in K, and T is the excitation temperature. The degeneracy depends only on the rotational state, J. Thus, $g_{1,3} = g_{2,3}$. We find:

$$\frac{I_{v=1-0\ S(1)}}{I_{v=2-1\ S(1)}} = \frac{A_{v=1-0\ S(1)}}{A_{v=2-1\ S(1)}} \frac{2.24\,\mu{\rm m}}{2.12\,\mu{\rm m}} \exp\left(\frac{E_{2,3} - E_{1,3}}{T}\right)$$
$$= 0.736 \exp\left(\frac{5594\ {\rm K}}{T}\right), \quad (4)$$

which gives a value of 198 at 1000 K and 5 at 3000 K. Similarly, we find $I_{v=1-0\ S(1)}/I_{v=1-0\ S(0)} \simeq 3-5$ for $T \sim 1000-3000$ K.

From these estimates, it is clear that a range of shock temperatures can reproduce the line ratios observed around T Tau N (Table 1). However, since the observations give us only lower limits to the line ratios, we are not able to constrain the shock temperature and thus the underlying physical parameters very well. We therefore turn to the total line flux. Shock models show that the H_2 $v = 1-0$ S(1) surface brightness in Fig. 2 can be produced in different density regions of the circumstellar material. The required density is tightly correlated with the impact velocity of the shock front. This means that the H_2 emission can arise in environments with pre-shock density of $n_{\rm H} \sim 10^4$ cm^{-3} if the shock velocity is ∼40−50 km s^{-1} while a shock front propagating at only ∼10 km s^{-1} is sufficient to excite the H_2 if the pre-shock density is $n_{\rm H} \sim 10^7$ cm^{-3} (L. E. Kristensen, private communication).

From models of T Tauri stars with disk and envelope masses resembling those of T Tau N, it is evident that the high density regime of $n_{\rm H} \sim 10^7$ cm^{-3} is associated with the upper layers of the disk while densities of $n_{\rm H} \sim 10^4$ cm^{-3} are found in the envelope and in a thin transition zone between the disk atmosphere and the outflow cavity, i.e. the cavity walls (Whitney et al. 2003; Crapsi et al. 2008). Independent of where the excitation takes place, the outflow or wind must impact the gas at a small angle, unless the disk is highly flared. Thus, the flow velocity must be much higher than the shock velocity, since it is only the velocity component perpendicular to the shock surface that contributes to the shock. Assuming an impact angle of 10°−20°, a flow velocity of 120−230 km s^{-1} is required to create a shock of 40 km s^{-1}. Such velocities are found in the collimated jets from T Tauri stars. However, the SED indicates that the cavity opening angle is large (∼47°, Table 2) and thus it is difficult to see how a collimated jet should be able to hit the cavity walls. On the other hand, a shock velocity of 10 km s^{-1} can be attained with a flow velocity of 30−60 km s^{-1} and an impact angle of 10°−20°. Such velocities may be found in a wide-angled low velocity wind characteristic of T Tauri stars (Bacciotti et al. 2000; Takami et al. 2006).

In summary, if shocks are the primary cause of the H_2 excitation, it seems more likely that they arise from the interaction of a wide-angled wind with the upper layers of a flared disk than with cavity walls carved in a circumstellar envelope. We cannot exclude that the H_2 excitation arises from the cavity walls, but this scenario seems to require that the high velocity jet in T Tau N be less collimated than in other sources.

5.2. Irradiation

We now turn to excitation process (ii), irradiation by UV-photons and X-rays (Fig. 5c). In their models of fluorescent excitation of H_2, Black & van Dishoeck (1987) find $I_{v=1-0\ S(1)}/I_{v=1-0\ S(0)} < 2.7$ and $I_{v=1-0\ S(1)}/I_{v=2-1\ S(1)} < 2.0$. This is incompatible with our data (Table 1) and shows that fluorescence alone cannot explain the observations. A thermal component is necessary in order to reproduce the line ratios. Le Petit et al. (2006) have shown that the ratio $I_{v=1-0\ S(1)}/I_{v=2-1\ S(1)}$ can be much larger than 2 in a photon-dominated region (PDR) if $n_H > 10^5$ cm^{-3} and the incident far-ultraviolet radiation field is stronger than $\sim 10^4$ times the average in the interstellar medium. In such high density regions, collisions of H_2 in vibrationally excited states resulting from fluorescence with atomic H tend to thermalize the rovibrational states. These conditions may very well apply to a dense circumstellar disk irradiated by the central star. The brightness of the $v = 1-0$ S(1) line in the model is found to be larger than $\sim 5 \times 10^{-4}$ erg s^{-1} cm^{-2} sr^{-1} in a PDR viewed face on (Le Petit et al. 2006), which is consistent with our data. The H_2 brightness around T Tau N is larger than this value out to distances of ~80 AU (Fig. 2). The H_2 emission may thus be caused by UV-irradiation from T Tau N creating a PDR at the dense surface of the disk. Such a PDR would create fluorescent H_2 lines in the UV and infrared H_2 lines composed of contributions from both fluorescence and thermal excitation. Walter et al. (2003) found extended fluorescent H_2 emission in the UV around T Tau N. This seems to support our conclusion. Herczeg et al. (2006), however, did not find fluorescent H_2 emission in the UV extending more than 0.″1 from T Tau N. Saucedo et al. (2003) reported fluorescent H_2 emission North-East and South-West of T Tau N at a distance of ≤50 AU, which is consistent with pumping by stellar Lyα emission. They do, however, find that the fluorescent line needs to be heated before being pumped and suggest that an outflow must be the heating mechanism.

Nomura et al. (2007) constructed models of H_2 emission from a disk irradiated by both X-rays and UV photons from a central T Tauri star. For a model with a 0.5 $M_\odot$, $T_{\rm eff} = 4000$ K central star with X-ray luminosity of $L_X \sim 10^{30}$ erg s^{-1} and UV excess like TW Hydrae, they find $v = 1-0$ S(1) line fluxes of $0.1-20 \times 10^{-15}$ erg s^{-1} cm^{-2}, depending on the size of the dust grains. When the grain size increases the high-temperature region in the disk shrinks and the line flux decreases. The $I_{v=1-0\ S(1)}/I_{v=2-1\ S(1)}$ ratio is always larger than 4 and can be as high as 50 if UV radiation dominates. In units of 10^{-14} erg s^{-1} cm^{-2}, the estimated flux in the $v = 1-0$ S(1) line for a model using small dust grains is found to be ~0.1 when only X-ray irradiation is considered, ~1.3 with only UV-irradiation and ~2.1 when both X-rays and UV-irradiation are included (Nomura et al. 2007). The estimated total flux from the disk around T Tau N is 1.8 on this scale, suggesting that X-rays alone are not sufficient to produce the observed H_2 emission. UV-photons seem to dominate the excitation but a combination of X-rays and UV-photons may be necessary in order to explain the H_2 flux as emission from a disk around T Tau N. Note that T Tau has an X-ray luminosity of $L_X = 3.5 \times 10^{31}$ erg s^{-1} (Güdel et al. 2007) and UV-luminosity of $L_{UV} = 3 \times 10^{33}$ erg s^{-1}, corresponding to a large UV-excess of 0.7 $L_\odot$ (Calvet et al. 2004).

It seems likely, then, that the UV-irradiation from T Tau N itself, with a possible X-ray contribution, is strong enough to produce the total H_2 flux we see around T Tau N. However, in their models, Nomura et al. (2007) find that most H_2 emission in the $v = 1-0$ S(1) line is emitted at a radius of 20 AU and that the emissivity decreases with increasing distance from the star. The presence of H_2 emission extending to ~100 AU around T Tau may be difficult to explain with models of irradiation. A possible way to solve this is if the disk is strongly flared. A large degree of flaring will allow more UV-photons to reach the outer parts of the disk, thus increasing the excitation in the outer regions.

5.2.1. Photoevaporation

If the disk is irradiated by UV photons and X-rays, a disk-wind may be powered by photoevaporation of the disk (Hollenbach et al. 1994; Johnstone et al. 1998; Störzer & Hollenbach 1999; Font et al. 2004). The high-energy radiation (EUV + X-rays) ionizes hydrogen at the disk surface and heats the gas to 10^4 K. EUV photons cannot penetrate the ionization front and X-rays heat only the inner disk and the surface layer (Nomura et al. 2007). FUV photons, which are not absorbed by atomic hydrogen but mainly by dust, penetrate much deeper and reach the disk surface. Here, they dissociate molecular hydrogen and heat the neutral gas to about 400–4000 K. If the thermal velocity of the neutral gas exceeds the escape velocity of the disk surface, the gas flows outward. The flow is initially cylindrical but is reoriented into a spherical flow by pressure gradients (Font et al. 2004). Deeper in this photon-dominated region, there is an H/H_2 transition layer below which the gas is molecular. The H_2 $v = 1-0$ S(1) line is emitted from the H/H_2 transition layer, which is close to the disk surface (Störzer & Hollenbach 1999). See Fig. 13 in Dullemond et al. (2007) for an illustration of the structure of a photoevaporative disk. Störzer & Hollenbach (1999) pointed out that the ionization structure in a PDR with photoevaporation may differ from a classical PDR because the material is not at rest. They also found that the H_2 $v = 1-0$ S(1) and $v = 2-1$ S(1) lines are mainly collisionally excited, and that fluorescence contributes only a small amount to the line intensities. The $I_{v=1-0\ S(1)}/I_{v=2-1\ S(1)}$ ratio is typically 5–10.

If the molecular hydrogen in the H/H_2 transition layer gets hot enough to overcome the escape velocity it may contribute to the gas flow away from the disk. This could explain the small blueshift of the line profile in Fig. 4.

5.2.2. Mass loss

It is interesting to consider the scale of the mass loss due to photoevaporation. A characteristic radius for thermal evaporation is (Dullemond et al. 2007):

$$r_g \sim 100\ \mathrm{AU} \left(\frac{T}{1000\ \mathrm{K}}\right)^{-1} \left(\frac{M_\star}{M_\odot}\right), \quad (5)$$

where the sound speed equals the escape speed. However, simulations have shown that evaporation is initiated at smaller radii than this analytical result suggests. That is, photoevaporation happens outside $r_{cr} > 0.15\, r_g$ (Dullemond et al. 2007). Using $M = 2\ M_\odot$ and $T = 10^4$ K as a typical temperature of the ionized gas, we find $r_{cr} \sim 3$ AU or about 20 mas. It thus seems very likely that the H_2 emission caused by irradiation is accompanied by a photoevaporative wind although it is not directly detected in these observations.

Hollenbach et al. (1994) derived an estimate for the hydrogen mass loss rate due to photoevaporation,

$$\dot{M}_{\rm wind} \simeq 4 \times 10^{-10} \left(\frac{\Phi}{10^{41}\ \mathrm{s}^{-1}}\right)^{1/2} \left(\frac{M_\star}{M_\odot}\right)^{1/2} M_\odot\ \mathrm{yr}^{-1}, \quad (6)$$

where Φ is the stellar ionizing flux. Alexander et al. (2005) found $\Phi \sim 10^{41}-10^{44}$ photons s^{-1} in five CTTs with ages of

around 10^6 years. Assuming that the ionizing flux of T Tau N also falls within this range, we estimate the mass loss rate to be 5×10^{-10}–2×10^{-8} $M_\odot$ yr^{-1}. The mass loss rate from a photoevaporative wind would thus be significantly smaller than the accretion rates inferred from SED modeling (Table 2), while the upper limit is similar to the observed accretion rate of $(1.4–5.9) \times 10^{-8}$ $M_\odot$ yr^{-1} (Beck et al. 2004). Since the accretion rate from the SED might be overestimated (Sect. 4) the photoevaporative wind may have a significant effect on the dispersal of the T Tau N disk at its present evolutionary state.

5.3. Other indicators

Two scenarios seem likely to explain the H_2 emission: shocks from a stellar wide-angle wind interacting with a flared disk, or irradiation from the central star onto the disk. The latter may or may not be accompanied by photoevaporative mass loss. The simplest way to distinguish between shock and PDR excitation is that the latter will create an atomic ionized layer giving rise to hydrogen recombination lines. Furthermore, a PDR will display strong emission from [OI] 63 μm, 145 μm and [CII] 158 μm as well as [FeII] 1.26 μm, 1.64 μm and [OI] 6300 Å and [SII] 6730 Å in high density regions. We examined the spatial distribution of the continuum-subtracted Brγ line to search for extended Brγ emission in comparison to the presumably pointlike PSF of the adjacent continuum. We did not find any conclusive evidence for any spatial extension of the Brγ line. This is consistent with Kasper et al. (2002), who found that extended Brγ emission, if any, is confined to within 6 AU of the star. This argues against the existence of an extended PDR.

On the other hand, van den Ancker et al. (1999) found strong [OI], [CII] and [FeII] lines which they were unable to fit with shock models. Although these data suffer from low spatial resolution (>20″), these findings suggest the presence of a PDR component. With 2″ resolution Solf & Böhm (1999) found a compact emission region in the optical [OI] and [SII] lines which is centered close to T Tau N and is characterized by near-zero radial velocities. Our SINFONI observations of the T Tau system included J-band data which are not presented here (see Gustafsson et al., in prep.). These measurements are centered on T Tau S and do not cover T Tau N. Nevertheless, the data show indirect evidence of strong [FeII] 1.26 μm and [OI] 1.13 μm emission close to or originating from T Tau N itself. In the J-band data, continuum emission from T Tau N is scattered into the field of view and we find [OI] and [FeII] emission with the same spatial distribution as the scattered light. We therefore believe that the emission originates in T Tau N. The [OI] line traces the ionization front (Marconi et al. 1998) and the presence of these lines indicates that a PDR contribution may be present after all.

One possible solution to reconcile these apparently contradictory observations is that a PDR exists but is confined to within ~6 AU from T Tau N. The infrared H_2 emission analysed here extends to much larger radii and would then be due to shocks. In any case, the emission seems to be linked to a nearly face-on disk. Future observations with high spectral and spatial resolution will be needed to confirm or disprove these suggestions. Such measurements should include deeper observations of the infrared H_2 lines to constrain the line ratios, spectrally resolved measurements of the velocity, a search for extended hydrogen recombination lines, and observations to spatially constrain the [OI], [FeII], [SII] and [CII] lines.

6. Implications for T Tau S

T Tau S is located at a projected distance of 0.″7 (~100 AU) south of T Tau N. The extent of the H_2 emission, as well as the SED modeling, indicate that the outer radius of the disk around T Tau N is 85–100 AU. Disks around stars in binary or multiple stellar systems will be truncated by their mutual gravitational influence. The size of the disk depends on the mass ratio of the stars and their separation. The disk size typically ranges from 0.3–0.4 times the separation for mass ratios of 1–0.3, even when the disk and orbital plane are not coplanar (Artymowicz & Lubow 1994; Larwood et al. 1996). If the true size of the disk around T Tau N is ~100 AU, the argumentation above implies that the orbital distance to T Tau S is ~300 AU and that the inclination of the orbit to the line-of-sight is ~20°.

If, on the one hand, T Tau S is located in front of T Tau N, UV irradiation from the 2.7 $M_\odot$ star T Tau Sa (Duchêne et al. 2006) could in principle contribute significantly to the H_2 excitation on the side of the T Tau N disk facing toward us. However, in that case the H_2 emission would be accompanied by extended Brγ emission as discussed in Sect. 5.3. This is not seen. On the other hand, if T Tau S is located behind T Tau N, the size of the disk indicates that it may very well contribute to the extinction of T Tau S. Given the small angular separation of T Tau Sa-Sb of ~0.″1 the disk around T Tau N would most likely obscure both Sa and Sb by an equal amount of material. Therefore, it does not help to explain why Sb is a normal T Tauri star and Sa shows the characteristics of an infrared companion (Dyck et al. 1982). The relative position of T Tau N and S and their outflows are the subjects of a subsequent paper (Gustafsson et al., in prep.).

7. Conclusions

We detect emission from the H_2 $v = 1–0$ S(1) rovibrational line at 2.12 μm in a ring-like structure very close to T Tau N. We find that the weak H_2 emission is most likely linked to a nearly face-on flared disk. Another possible solution is that the H_2 emission originates from shocks impacting on the lower density walls of an envelope cavity. This scenario, however, requires that the high velocity jet in T Tau N be less collimated than in other T Tauri stars. The radius of the disk is ~85–100 AU, based on SED modeling and the extent of the H_2 emission. The velocity in the vicinity of T Tau N is consistent with the rest velocity of the star to within the errors. Both shocks associated with a wide-angle wind impinging on the disk and UV + X-ray irradiation from the central star onto the disk are plausible excitation mechanisms which can reproduce the H_2 flux. Both these mechanisms require a substantial disk around T Tau N. However, models and observations indicate that irradiation from the central star cannot excite H_2 at radii much larger than 20 AU. Thus, the most likely excitation mechanism of H_2 is that of a wide-angle wind impinging on a flared disk. A PDR created by irradiation may exist within ~6 AU from T Tau N.

Acknowledgements. We would like to thank L.E. Kristensen for providing data from numerical shock models and J. Sauter for modeling disk and envelope densities. We are also grateful to Reinhard Mundt and Cornelis Dullemond for fruitful discussions.

References

Akeson, R. L., Koerner, D. W., & Jensen, E. L. N. 1998, ApJ, 505, 358
Akeson, R. L., Ciardi, D. R., van Belle, G. T., & Creech-Eakman, M. J. 2002, ApJ, 566, 1124
Alexander, R. D., Clarke, C. J., & Pringle, J. E. 2005, MNRAS, 358, 283
Andrews, S. M., & Williams, J. P. 2005, ApJ, 631, 1134

Artymowicz, P., & Lubow, S. H. 1994, ApJ, 421, 651
Bacciotti, F., Mundt, R., Ray, T. P., et al. 2000, ApJ, 537, L49
Bary, J. S., Weintraub, D. A., & Kastner, J. H. 2003, ApJ, 586, 1136
Bary, J. S., Weintraub, D. A., Shukla, S. J., Leisenring, J. M., & Kastner, J. H. 2008, ApJ, 678, 1088
Beck, T. L., McGregor, P. J., Takami, M., & Pyo, T.-S. 2008, ApJ, 676, 472
Beck, T. L., Prato, L., & Simon, M. 2001, ApJ, 551, 1031
Beck, T. L., Schaefer, G. H., Simon, M., et al. 2004, ApJ, 614, 235
Beckwith, S. V. W., & Sargent, A. I. 1991, ApJ, 381, 250
Black, J. H., & van Dishoeck, E. F. 1987, ApJ, 322, 412
Calvet, N., Muzerolle, J., Briceño, C., et al. 2004, AJ, 128, 1294
Campins, H., Rieke, G. H., & Lebofsky, M. J. 1985, AJ, 90, 896
Carmona, A., van den Ancker, M. E., Henning, T., et al. 2008, A&A, 478, 795
Chen, H., Bally, J., O'dell, C. R., et al. 1998, ApJ, 492, L173
Crapsi, A., van Dishoeck, E. F., Hogerheijde, M. R., Pontoppidan, K. M., & Dullemond, C. P. 2008, A&A, 486, 245
Duchêne, G., Ghez, A. M., McCabe, C., & Ceccarelli, C. 2005, ApJ, 628, 832
Duchêne, G., Beust, H., Adjali, F., Konopacky, Q. M., & Ghez, A. M. 2006, A&A, 457, L9
Dullemond, C. P., Hollenbach, D., Kamp, I., & D'Alessio, P. 2007, in Protostars and Planets V, ed. B. Reipurth, D. Jewitt, & K. Keil, 555
Dyck, H. M., Simon, T., & Zuckerman, B. 1982, ApJ, 255, L103
Eisenhauer, F., Abuter, R., Bickert, K., et al. 2003, in Presented at the Society of Photo-Optical Instrumentation Engineers (SPIE) Conference, Instrument Design and Performance for Optical/Infrared Ground-based Telescopes, ed. M. Iye, & A. F. M. Moorwood, Proc. SPIE, 4841, 1548
Font, A. S., McCarthy, I. G., Johnstone, D., & Ballantyne, D. R. 2004, ApJ, 607, 890
Ghez, A. M., Neugebauer, G., Gorham, P. W., et al. 1991, AJ, 102, 2066
Güdel, M., Skinner, S. L., Mel'Nikov, S. Y., et al. 2007, A&A, 468, 529
Hartmann, L., Hewett, R., Stahler, S., & Mathieu, R. D. 1986, ApJ, 309, 275
Herbst, T. M., Robberto, M., & Beckwith, S. V. W. 1997, AJ, 114, 744
Herbst, T. M., Hartung, M., Kasper, M. E., Leinert, C., & Ratzka, T. 2007, AJ, 134, 359
Herczeg, G. J., Linsky, J. L., Walter, F. M., Gahm, G. F., & Johns-Krull, C. M. 2006, ApJS, 165, 256
Hogerheijde, M. R., van Langevelde, H. J., Mundy, L. G., Blake, G. A., & van Dishoeck, E. F. 1997, ApJ, 490, L99
Hollenbach, D., Johnstone, D., Lizano, S., & Shu, F. 1994, ApJ, 428, 654
Itoh, Y., Sugitani, K., Ogura, K., & Tamura, M. 2003, PASJ, 55, L77
Johnstone, D., Hollenbach, D., & Bally, J. 1998, ApJ, 499, 758
Kasper, M. E., Feldt, M., Herbst, T. M., et al. 2002, ApJ, 568, 267
Kenyon, S. J., & Hartmann, L. 1995, ApJS, 101, 117
Lahuis, F., van Dishoeck, E. F., Blake, G. A., et al. 2007, ApJ, 665, 492
Larwood, J. D., Nelson, R. P., Papaloizou, J. C. B., & Terquem, C. 1996, MNRAS, 282, 597
Le Petit, F., Nehmé, C., Le Bourlot, J., & Roueff, E. 2006, ApJS, 164, 506
Marconi, A., Testi, L., Natta, A., & Walmsley, C. M. 1998, A&A, 330, 696
Mayama, S., Tamura, M., Hayashi, M., et al. 2006, PASJ, 58, 375
McCabe, C., Duchêne, G., & Ghez, A. M. 2002, ApJ, 575, 974
Momose, M., Ohashi, N., Kawabe, R., Hayashi, M., & Nakano, T. 1996, ApJ, 470, 1001
Nomura, H., Aikawa, Y., Tsujimoto, M., Nakagawa, Y., & Millar, T. J. 2007, ApJ, 661, 334
Ramsay Howat, S. K., & Greaves, J. S. 2007, MNRAS, 379, 1658
Robitaille, T. P., Whitney, B. A., Indebetouw, R., & Wood, K. 2007, ApJS, 169, 328
Saucedo, J., Calvet, N., Hartmann, L., & Raymond, J. 2003, ApJ, 591, 275
Solf, J., & Böhm, K.-H. 1999, ApJ, 523, 709
Stapelfeldt, K. R., Burrows, C. J., Krist, J. E., et al. 1998, ApJ, 508, 736
Störzer, H., & Hollenbach, D. 1999, ApJ, 515, 669
Takami, M., Chrysostomou, A., Ray, T. P., et al. 2006, ApJ, 641, 357
van den Ancker, M. E., Wesselius, P. R., Tielens, A. G. G. M., van Dishoeck, E. F., & Spinoglio, L. 1999, A&A, 348, 877
Walter, F. M., Herczeg, G., Brown, A., et al. 2003, AJ, 126, 3076
Weaver, W. B., & Jones, G. 1992, ApJS, 78, 239
Weinberger, A. J., Becklin, E. E., Schneider, G., et al. 2002, ApJ, 566, 409
Weintraub, D. A., Bary, J. S., Kastner, J. H., Shukla, S. J., & Chynoweth, K. 2005, BAAS, 37, 1165
White, R. J., & Ghez, A. M. 2001, ApJ, 556, 265
Whitney, B. A., Wood, K., Bjorkman, J. E., & Cohen, M. 2003, ApJ, 598, 1079